Research Article

Structural, optical and electrical properties of Cu:MnO_2 nanostructured thin films for glucose sensitivity measurements

Muslima Zahan[1] · **Jiban Podder**[1]

Received: 6 January 2020 / Accepted: 5 February 2020 / Published online: 12 February 2020

Abstract
In the present investigation, pure MnO_2 and Cu doped MnO_2 (Cu:MnO_2) thin films were successfully prepared by the spray pyrolysis deposition technique. Different Cu concentrations were used to analyze the morphological, structural, optical, electrical properties and as well glucose sensitivity measurement has been performed. MnO_2 doped with Cu induces microstructure and is set in the lattice by keeping Mn^{+2} leading to the micro spherical shape of the samples highlighted from a scanning electron microscope. X-ray diffraction analysis has confirmed the tetragonal MnO_2 crystal structure with α-phase. The crystallite size, crystal structure, texture, and nanoparticle formation in MnO_2 films have been influenced by Cu dopant. The maximum optical transmittance is found to be about 83%. The energy band gap associated with the allowed direct transition is found to increase from 3.82 to 3.96 eV with increasing Cu doping concentration up to 4 at%. Glucose sensitivity was measured by the four-probe technique. Notably, 4 at% Cu:MnO_2 films have demonstrated the superior sensing ability of glucose of 29%.

Keywords Thin films · Cu:MnO_2 · Nanoparticles · Porous structure · Band gap energy · Biosensors

1 Introduction

Nanostructured manganese dioxide (MnO_2) is a promising transition metal oxide for its admirable chemical stability, transparency, low toxicity, low cost, functional biocompatibility, excellent adsorption capacity, catalytic properties, and widespread availability. Thin films of MnO_2 are widely used in bio-sensors [1, 2] gas sensors [3], catalysis, electromagnetic wave-absorbing layers, and high-performance electrochemical electrodes and energy storage [4–6]. The presence of the dopants plays a crucial role in improving the chemical and physical properties of MnO_2 thin films. A good number of research work have been done on the synthesis and characterization of Al, Ag, Co, and Cr, etc. doped MnO_2 thin films [7–10]. Supplementary to these metals, Cu has a great deal of diligence dopant because of its low cost, good electrical conductivity, non-toxicity and environmentally friendly nature [11]. Different methods have been engaged to fabricate MnO_2 thin films viz hydrothermal technique [12], Sol–gel technique [13], electrochemical deposition method [14], reduction process [15], and spray pyrolysis technique [16, 17]. Very few reports are available on Cu doped MnO_2 with a well discussion on gas sensing and biosensing application.

Now a days, the determination of glucose is important in clinical applications as well as in the area of food, medical, pharmaceutical, and environmental analyses. Thin-film biosensors have been mainly based on potentiometric or amperometric detection modes. It has been shown that potentiometric sensors can measure glucose concentrations of 10 μM or higher [18] Although they exhibit high sensitivities but they have shortcomings, such as limited operating conditions, short lifetimes, instability, high cost, and frequent maintenance requirements. Recently, an

✉ Jiban Podder, jpodder59@gmail.com | [1]Department of Physics, Bangladesh University of Engineering and Technology, Dhaka 1000, Bangladesh.

SN Applied Sciences (2020) 2:385 | https://doi.org/10.1007/s42452-020-2191-8

advanced method for glucose equipped with MnO_2 has been studied, known as a conductometric mode. Against the mechanical point of view, it is crucially important that conductometric biosensors are suitable for great performance using inexpensive thin-film technology. MnO_2-based glucose sensors have shown immense sensitivity and unelevated detection limits [19]. Due to high sensitivity and large surface area, MnO_2 nanoparticles are suitable for higher glucose sensing detection. It is manifest that nanostructure is advantageous for sensing because of adequate ion and electron transport pathways. Copper (Cu) ions have long recognized for human health. However, there are few works have been reported on nanostructured Cu:MnO_2 thin films. Hence to explore and develop the performance of Cu:MnO_2 through effective routes for achieving high performance of glucose sensing abilities, further study is essential. Based on the above considerations, we have developed an electrical method for directly use of nanostructured Cu:MO_2 films as the electrode for glucose sensing containing a little amount, quiet operation, fast sensing current, etc. This technique has to turn out for an effective technique for the fast and precise determination of glucose sensitivity. The motivation of this work is to prepare spray pyrolyzed nanostructured pure and Cu doped α-MnO_2 thin film and to see the effect of Cu concentrations on the optical morphological, structural, and electrical properties of α-MnO_2 thin films favorable for optoelectronics and biosensing applications.

2 Experimental

To fabricate the Cu doped MnO_2 thin films, manganese (II) acetate tetra-hydrate (Mn $(CH_3COO)_2{\cdot}4H_2O$), molecular weight 245.085 gm/mol, purity 99%, Merck, Germany, and copper (II) acetate monohydrate ($Cu(CH_3COO)_2{\cdot}H_2O$), molecular weight 199.649 gm/mol, purity 99%, Merck, Germany, were used as precursor materials. The spray solutions were prepared by dissolving $Mn(CH_3COO)_2{\cdot}4H_2O$ and $Cu(CH_3COO)_2{\cdot}H_2O$ in 100 mL of double-distilled water (DDW). Cu doped MnO_2 thin films were prepared with 2, 4, and 6 at% Cu concentrations. Few drops of ethanol (C_2H_5OH) and hydrochloric acid (HCl) were added to keep the pH value at 6. The precursor solution was then stirred with a magnetic stirrer at room temperature for about 1 h to form a homogeneous solution. The solution was then filtered and sprayed through a fine bore onto the pre-heated microscopic glass substrates for 20 min deposition time. The temperature of the substrate was kept constant at 350 °C and monitored with a high-temperature infrared pyrometer during film deposition. The distance between the spray nozzle and the substrate was kept at 25 cm. The pressure of the carrier gas as the air was kept fixed at 0.5 bar and spray rate was maintained at 0.5 mL min^{-1} throughout the deposition of the film. D-glucose ($C_6H_{12}O_6$) and sodium hydro oxide (NaOH) were used as precursors for sensitivity measurements.

Surface morphology, compositional analysis, structural, optical and electrical properties of the synthesized films were analyzed using the Field Emission Scanning Electron Microscope (FESEM), Model: JSM-7600F, operated at 20 kV), Energy dispersive X-Ray analysis (EDAX) spectra, X-ray diffractometer (10°–90° with a CuKα radiation source of 1.54056 Å), UV–Vis spectrophotometer (UV-2600, Pc: UV–Vis–NIR; Shimadzu) and four-probe technique, respectively.

The electrical measurements were carried out by the four-probe method. The current was supplied through the outer two probes and the voltage drop was measured between the inner two probes. The Hall Effect measurements were performed at room temperature by a Hall effect measuring apparatus (ECOPIA HMS-5000, USA) under magnetic field 0.54 T and current 10 mA.

Glucose sensitivity was also measured by the four-probe method. For Glucose sensing measurements, two electrodes were used: one as reference (Zn-plate, positive electrode) and the other as counter (Cu-plate, negative electrode). Here the deposited thin film acted as the sensing element, which was placed under four probe systems. In our experiment we measured the current through the as-deposited thin films with and without glucose solutions to check the response of the film. NaOH was used to release the hydroxyl ions (OH^-) and to accelerate ionic exchange mechanism. The reaction mechanism has been explained in details in the experimental section.

3 Results and discussion

3.1 Surface morphology

The surface morphology of pure and 2 at%, 4 at%, and 6 at% Cu-doped MnO_2 thin films are studied by taking FE-SEM images under × 100,000 magnification. 100 nm scale bar length revealed in Fig. 1a–d.

Figure 1a reveals a granular surface of porous structures and orderless distribution of grains with round shapes. Cu doped MnO_2 films display a different morphology compared with MnO_2. The incorporation of Cu ions (either + 2 or + 1) into the lattice of MnO_2 films greatly affects the morphological feature and porous nature. For 2 at% Cu doped MnO_2 film, the grains seem to be agglomerated and the surface is covered with dense and homogeneously distributed grains supplementary in Fig. 1b. In Fig. 1c, d, as the Cu concentration is increased to 4 and 6 at%, the interior of the microspherical MnO_2 films is collapsed and

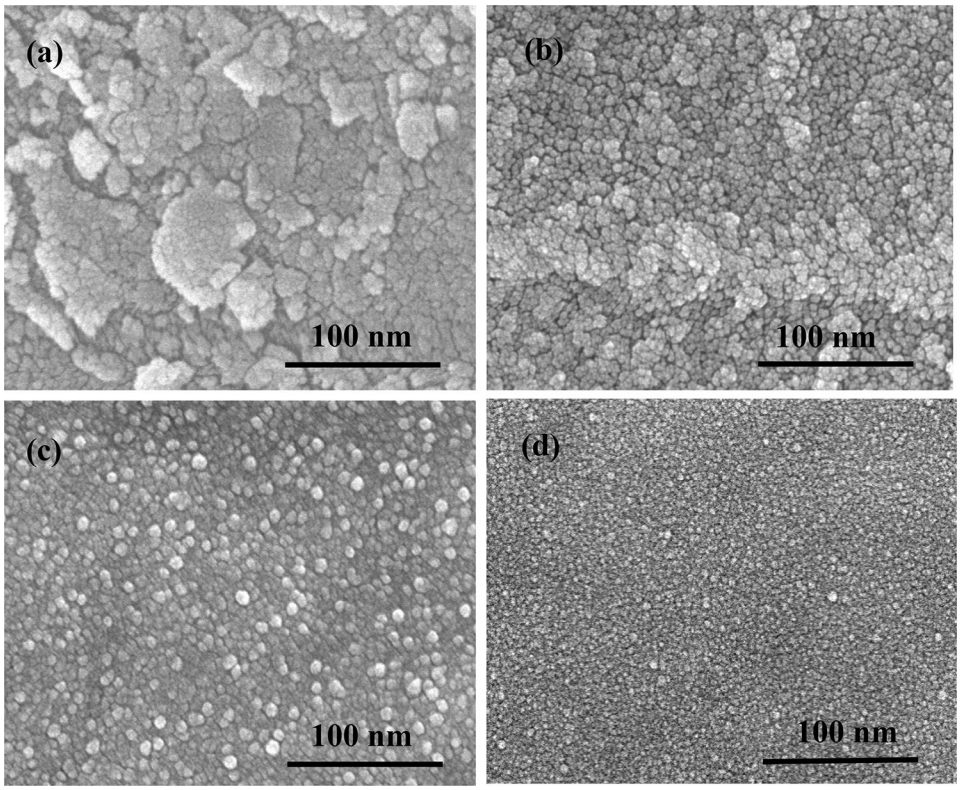

Fig. 1 FE-SEM images of **a** pure MnO_2, **b** 2 **c** 4 and **d** 6 at% Cu doped MnO_2 thin films

Table 1 EDAX report of pure MnO_2 and Cu doped MnO_2 thin films

Sample name	at% of elements		
	Cu	Mn	O
Pure MnO_2	0.00	31.04	68.96
2 at% Cu doped MnO_2	9.92	32.14	57.94
4 at% Cu doped MnO_2	11.05	29.78	59.17
6 at% Cu doped MnO_2	13.14	28.50	58.36

the grains are broken. The reason is that the presence of Cu^{+2} may have a tremendous effect on MnO_2 nanospheres, pointing to the formation of spherical structure.

Hence Cu behaves as an interstitial dopant with high solubility in MnO_2. When Cu solubility limit is reached, nucleation occurs into the surface of MnO_2 nanocrystals and yields phase shifts followed by the reduction of Cu^{+1} to Cu^{+0}. Cu impurities exhibited a high solubility limit in MnO_2 up to 4 at% nearly saturating the nanocrystals. Additionally, the solubility limit is considerable affection for the possible side effects in nanocrystals. The size of MnO_2 is decreased for the increase of the Cu/Mn ratio. A low Cu/Mn ratio indicates that few Cu impurities are present in each MnO_2 nanocrystal [20].

EDAX analysis confirmed the elements of the compositions of pure MnO_2 and Cu doped MnO_2 thin films. The EDAX reports are displayed in Table 1. EDAX data have been collected at various points on the scan area. EDAX data support the uniformity of the synthetic distribution of the prepared thin films. Amount of Mn reduces with the increment of Cu concentration in Cu doped MnO_2 thin films. The EDAX data supported the logical substitution of Mn caused by Cu doping (Fig. 2).

3.2 Structural characterization

Figure 3a–d depicts the X-ray diffraction patterns of pure MnO_2 and 2, 4 and 6 at% Cu doped MnO_2 thin films. The incorporation of Cu into the MnO_2 lattice shows a vital aspect in the structure of the films. The diffraction peaks of pure and Cu doped MnO_2 corresponds to α-phase having tetragonal crystal structure up to 4 at% Cu doping. Some additional peaks are observed for the 6 at% Cu doped MnO_2 thin film, which may due to the partial reduction of Mn^{+4} and Cu^{+2} from surface sites given forming Mn^{+3} and Cu^{+}. All the patterns are polycrystalline with preferential orientation along (400), (211) and (301) plane at $2\theta = 32.5°$, 35.9° and 43.5°, respectively which were matched with JCPDS data, card no. 44-0141. The additional peaks are due to the δ-MnO_2 phase along (001), and (111) plane at $2\theta° = 12.4°$, 40° (JCPDS no. 44-0142). The crystalline size was measured by Debye–Scherrer formula [21, 22] as follows:

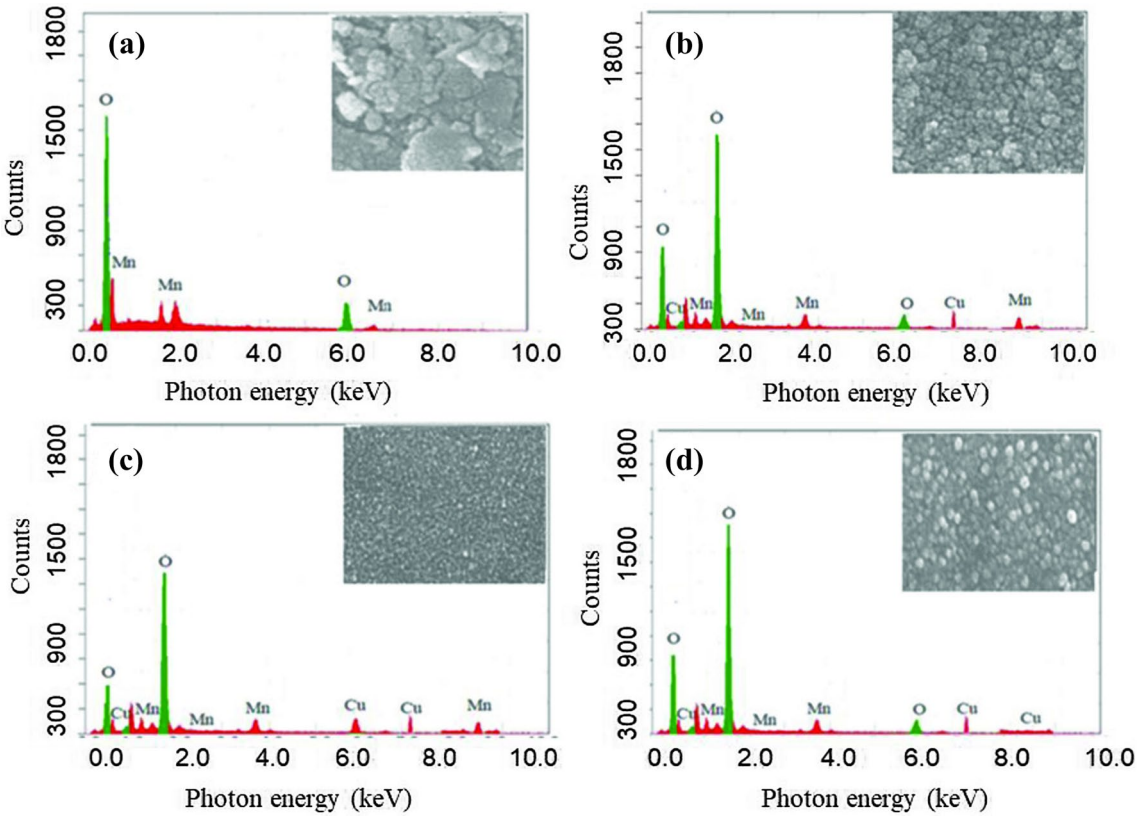

Fig. 2 EDAX of **a** pure MnO_2, **b** 2, **c** 4, and **d** 6 at% Cu doped MnO_2 thin films

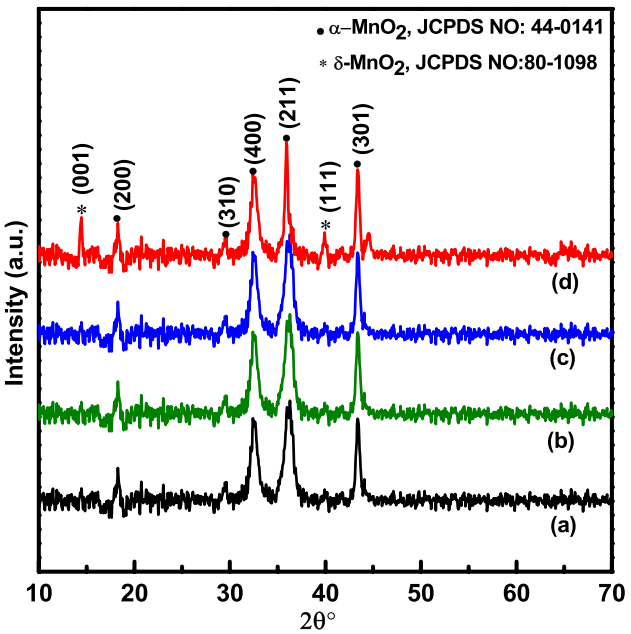

Fig. 3 XRD pattern of **a** pure MnO_2, **b** 2, **c** 4 and **d** 6 at% Cu doped MnO_2 thin films

$$<D> = \frac{0.9\lambda}{\beta \cos\theta} \quad (1)$$

where D is indicated average crystalline size in (Å), shape factor value is taken as 0.9, λ is the wavelength of X-ray radiation spectra, β is the full width half maximum (FWHM) after making appropriate base correction and θ is the most dominate diffraction angle at the position of the peak maximum. Strain (ε) is due to the fractional shift in length and the displacement of crystal momentum lines per unit volume, and dislocation density (δ) were calculated from the following equation [21, 22].

$$\varepsilon = \frac{\beta \cos\theta}{4} \quad (2)$$

$$\delta = \frac{1}{D^2} \quad (3)$$

The effect of Cu doping on particle size, dislocation density and strain of MnO_2 films on the most preferential (211) plane are shown in Table 2. Crystallite size reduces from 25 to 12 nm with the increase of Cu concentration from 2 to 6 at% in MnO_2 thin films. Dislocation density and strain increase by rising of Cu concentration in MnO_2 films. It may be because of the re-crystallization and increase of

Table 2 Effect of Cu concentration on structural parameters of MnO_2 thin films

Sample name	Crystallite size (nm)	Micro strain ($\times 10^{-4}$)	Dislocation density (lines/nm^2) $\times 10^{-3}$
Pure MnO_2	25	1.4	1.65
2 at% Cu:MnO_2	18	1.8	2.94
4 at% Cu:MnO_2	15	2.3	4.54
6 at% Cu:MnO_2	12	2.9	6.81

defect states in the lattice MnO_2 caused by the increase of Cu doping. Crystallite size is an important parameter of a material to be useful in gas and biosensing applications. Smaller crystallite size shows better gas sensitivity [20]. It is mentioned that the doping of Cu into MnO_2 may improve the gas and biosensing properties of MnO_2.

3.3 Optical properties

In view of analysis the effect of Cu concentrations onto MnO_2 over the optical properties, the transmission, reflectance spectra and bandgap have been studied. Figure 4a shows the optical transmittance spectra of pure MnO_2 and 2, 4 and 6 at% Cu doped MnO_2 thin films varying with a spectral range from 200 to 1100 nm. It is observed that the transmittance of the prepared films increases gradually with increasing Cu content in the visible–near-infrared region (400–800 nm) and the maximum transmittance is observed about 83% in 4 at% Cu doped MnO_2 thin film. The increase of transmittance with increasing Cu concentration may refer to the effects of excess charge carrier for the shake of Cu doping that is attributed to the improvement in a stoichiometry of the films. Transmittance decreases at 6 at% Cu doping in the IR region (800–1100 nm) which may be due to the transformation of the crystalline phase of MnO_2 as revealed by the XRD pattern shown in Fig. 3d.

It can be noticed that the low percentage of transmittance is found about 4–22% in the wavelength range 200–300 nm which may for absorption of light of the excitation electrons from valence band (VB) to conduction band (CB). It is also observed that thin films exhibited a blue shift into the absorption onset at 400 nm. This absorption is associated with $O^{-2} \rightarrow Mn^{+4}$ charge transfer, related to electron agitation from the valence band to the conduction band. The blueshift in the absorption spectrum is mainly attributed to the confinement of charge carriers in the porous surface of the MnO_2 film.

The thickness of the film is measured by the multiple-beam Fizeau fringe method. In this method two reflecting surfaces are brought into close proximity to produce interference fringes. The fringe spacing and fringe displacement across the steps are measured and used to calculate the film thickness. The displacement 'b' of the fringe system across the film-substrate step was measured to calculate the film thickness (t), using the relation

$$t = \frac{\text{step height}}{\text{fringe} - \text{spacing}} \frac{\lambda}{2} \quad (4)$$

where λ is the wavelength of the monochromatic light (sodium light, λ = 589.592 nm).

The calculated thickness increases as 285, 298, 303 and 317 nm with increasing Cu concentration as 0, 2, 4 and 6 at%.

Figure 4b shows the Tauc relation, $(\alpha h\nu)^2$ vs. photon energy ($h\nu$) for determination of optical band gap (E_g) related to the allowed direct transition of pure and 2, 4 and 6 at% Cu:MnO_2 thin films. The E_g of the films varies

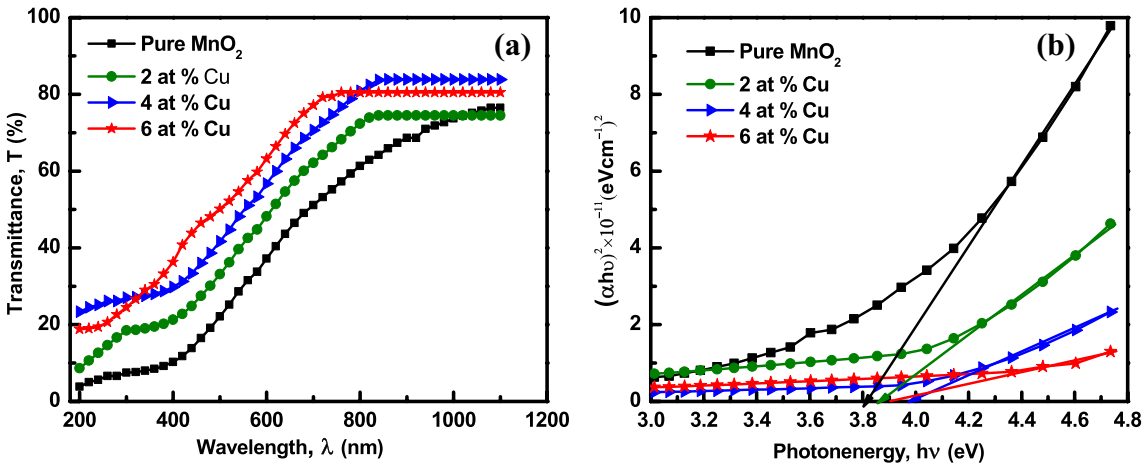

Fig. 4 **a** Wavelength versus optical transmittance spectra and **b** photon energy versus $(\alpha h\nu)^2$ of pure MnO_2 and 2, 4 and 6 at% Cu doped MnO_2 thin films

between 3.82 to 3.96 eV employing a gradual increment of Cu from 0 to 4 at%, which indicated that incorporation of a little amount of Cu affects the optical band transition and this may for the blue shift. A decrease in E_g with the increase of 6 at% Cu concentration is observed which is associated with the change in crystal structure from α to δ phase of MnO_2. Similar variations of the E_g value of MnO_2 have been reported by some other workers [20, 23]. The reduction of E_g in higher Cu concentration may due to redshift which interpreted in terms of the sp-d exchange interaction among the band electrons and localized d electrons of the Mn^{4+} ions and Cu + ions give rise to a negative and a positive correction to conduction and valence band edges is obtained by s-p and p-d exchange interactions governing to the increase of E_g. [24]. The thickness of the films affect the optical properties of the films. The optical parameters such as optical band gap, refractive index, extinction coefficient etc. are the key factor to determine the quality of the films. In the present work extinction coefficient (k) and refractive index (n) were calculated using the following relation:

$$k = \frac{\alpha\lambda}{4\pi} \text{ and } n = \frac{(1+R)}{(1-R)} + \sqrt{\left[\left\{\frac{4R}{(1-R)^2}\right\} - k^2\right]} \quad (5)$$

where α is absorption coefficient and R is reflectance. Table 3 shows the optical parameters of MnO_2 thin films variation with film thickness due to the effect of Cu concentrations.

Table 3 show that Optical band gap, refractive index and extinction coefficient values increase with increasing film thickness up to 4 at% Cu doping and then started to increase. These obtained values satisfy with other works [7, 10, 11]. Figure 5 displays the relation between bandgap and reflectance spectroscopy which indicates the effect of Cu dopant on the band structure in terms of Kubelka–Munk (K–M) function. The K–M function is based on the equation, $F(R) = \frac{(1-R)^2}{2R}$; where R is the reflectance; F(R) is propotional to the absorption coefficient. The obtained curves reveal parabolic band edges that depend on the photon energy and obey Urbachs rule that has been discussed in our previous work [25].

Table 3 Effect of film thickness on optical properties of Cu:MnO_2 thin films

Cu concentration (at%)	Film thickness (nm)	Optical bandgap (eV)	Refractive index	Extinction coefficient
0	285	3.82	2.8	1.3
2	298	3.89	2.5	0.9
4	303	3.99	2.3	0.6
6	317	3.96	2.4	0.8

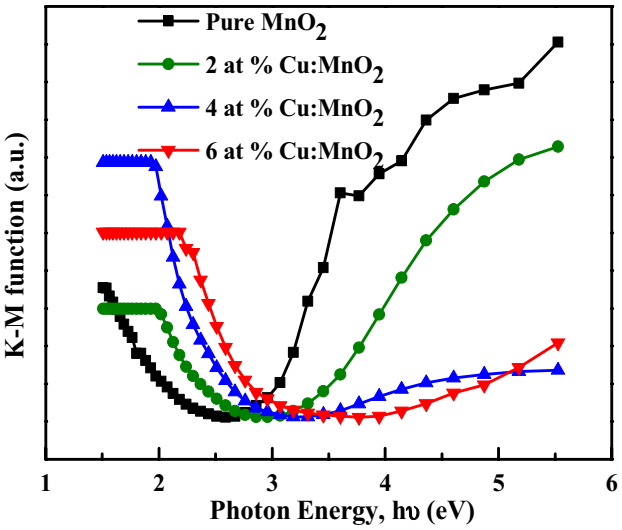

Fig. 5 A plot of bandgap versus K–M function

The lower edge shown in the figure is due to transitions between extended and localized states whose shape and magnitude trust in the purity and preparation conditions. The dopant level emerged between the valence band and the conduction band when Cu ions are assimilated into the MnO_2 lattice that results in shifting the absorbance edge to the visible region. These results let out that the small amount of Cu might be incorporated into the MnO_2 lattice.

3.4 Electrical properties

The variation of electrical resistivity with temperature ranging from 27 to 150 °C for pure and 2, 4 and 6 at% Cu doped MnO_2 thin films are shown in Fig. 6a. It is noticed that resistivity contracts with the rise of temperature. This type of variation indicates the semiconducting behavior of the films. The resistivity devaluates with expanding of Cu concentrations. Oxygen adaption and desertion may occur into a polycrystalline oxide semiconductor at all temperatures when the heat is treated in air. The oxygen decomposition process into the deposited films crops up the decrease in electrical resistivity. Figure 6b shows that Hall mobility and carrier concentration increases with the rise of Cu concentrations in Cu doped MnO_2 thin films. The increase of carrier concentration with some contribution from the increase of mobility leads to relatively low resistivity. The Hall coefficient, carrier concentration and mobility change with film thickness and composition of the films. The Hall mobility increases with Cu doping concentration as well as thickness due to the lower effective mean free path of conduction carriers that occurred by scattering from the surface of the film. The increase of Hall mobility indicates that shallow acceptor levels exist

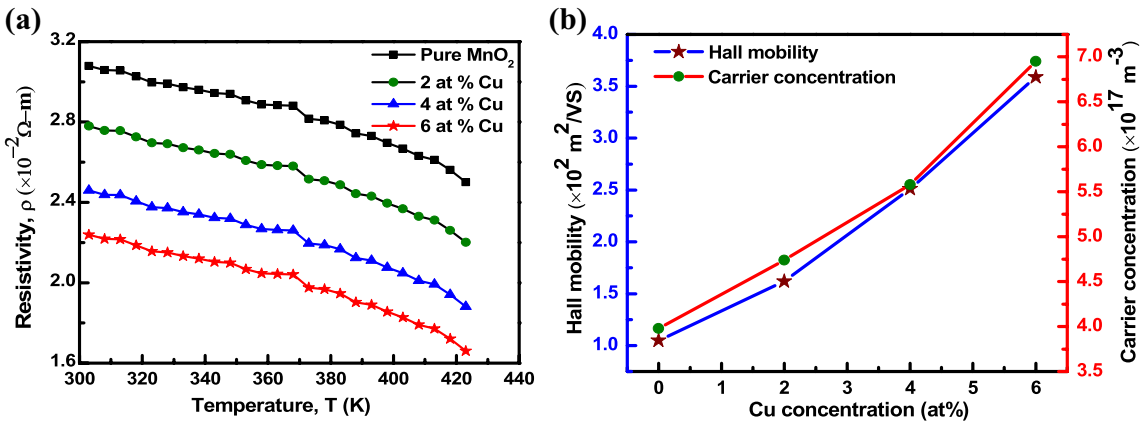

Fig. 6 **a** Variation of electrical resistivity with temperature for pure and Cu doped MnO_2 thin films **b** Variations in Hall mobility and carrier concentration with Cu concentration

in Cu:MnO_2 films due to stoichiometric defects. Also the increase of carrier concentration with increase of Cu doping and thickness for all compositions are attributed to lower defect density and less grain boundary scattering The increase of carrier concentration with increase of Cu concentration is probably due to creation of more acceptor levels with addition of Cu.

3.5 Glucose sensitivity measurement

The sensing ability of the prepared thin films concerning glucose ($C_6H_{12}O_6$) was evaluated by the four-probe method. In this method, two electrodes were used: one as reference (Zn-plate, positive electrode) and the other one as counter (Cu-plate, negative electrode). Here the deposited thin film acted as the sensing element, which was placed under four probe systems.The key factor in enhancing sensing ability is a fast electron transfer between the MnO_2 layer and the substrate to improve electron collection. In our experiment we measured the current through the as-deposited thin films with and without glucose solutions to check the response of the film. In the present work, 0.5 M $C_6H_{12}O_6$ solution with 0.2 M NaOH and a constant supply voltage of + 65 V were used for the sensitivity measurement. NaOH was used to release the hydroxyl ions (OH–) and to accelerate ionic exchange mechanism. Glucose sensing depends on the air oxidation of glucose molecules on the surface of the film layer and decomposition into glucono lactone ($C_6H_{10}O_6$) and hydrogen peroxide. Oxidation of glucose molecules on the surface of the film results in hydrogen peroxide molecules that pass through the porous thin film and adsorb on the surface of the counter electrode layer. Due to the oxidation–reduction of hydrogen peroxide molecules, the surface area increases the speed of the reaction and the output current increased. The addition of NaOH is also responsible for increasing the current to reach a stable state as glucose and OH^- molecules are adsorbed in the film surface. The possible chemical reactions are given as:

$$C_6H_{12}O_6 + H_2O + O_2 \rightarrow C_6H_{10}O_6 + H_2O_2$$
$$H_2O_2 \rightarrow O_2 + 2H^+ + 2e^-$$
$$NaOH \rightarrow Na^+ + OH^-$$
$$C_6H_{12}O_6 + H_2O + NaOH \rightarrow C_6H_{10}O_6 + O_2 + H^+ + 2e^-$$

The electrons produced in those reactions are transferred through the film layer. The porous structure of the film gives the ability for the NaOH molecules to adsorb on the surface of the counter electrode layer. The prepared thin films were examined for sensing the various concentrations of the glucose solution.

Figure 7 shows the resulted sensing current at 0.05, 0.1, 0.3, 0.5 and 1 mol/L glucose concentrations of pure MnO_2

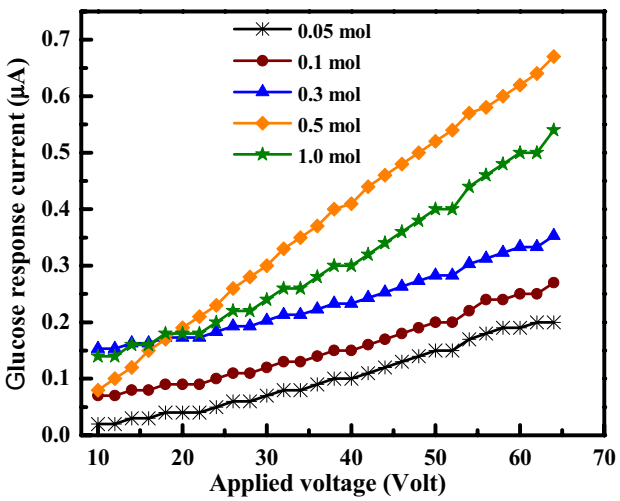

Fig. 7 Sensing current at (0.05, 0.1, 0.3, 0.5 and 1) mol/L glucose concentrations

thin films respectively. The obtained curves shown in Fig. 7 demonstrate the redox (oxidation–reduction) peak indicating the redox reaction of ion and electron exchange with the conductive solution. The increase of current with increasing glucose concentration may due to increase of oxidation by enhancing anode and cathode current. This increase of oxidation of glucose products glucono lactone. It was observed that the sensing current increased with the glucose concentration up to 0.5 mol/L and then started to decrease. The reason for the decrease in sensing current is that at high concentration, most of the active sites on the film surface area covered by glucose molecules and so the current response is reduced. The current increased steeply with increasing time to reach a stable state. We conceive that, since the adherence of the MnO_2 layer into the substrate was very strong, Cu–O–Mn bonds likely formed at the interface between the substrate and the MnO_2, which probably facilitated electron transfer across the interface, to cause a high current response. The sensor (Cu:MnO_2 film) has fast rise time which means that the oxygen ions at the film surface may immediately interact and bond with the glucose ($C_6H_{12}O_6$) molecules, this fast interaction provides a large number of charge carriers which caused the sharp rise of the sensing current.

Figure 8a–d shows the response time of pure MnO_2 and 2, 4 and 6 at% Cu doped MnO_2 thin films electrode as 1.13 s and 1.06, 0.99 and 1.02 s respectively which may be due to the incorporation of Cu into MnO_2, the Cu:MnO_2 may own more active sites for the detecting of glucose, displaying a shorter time for the detecting of glucose. Glucose response (S) of the sensor is defined as the ratio of change in the current of the sensor on the exposure of target to the sensing current in ambient air (at the same operating conditions).

The following relation was used to calculate the glucose response of the prepared film:

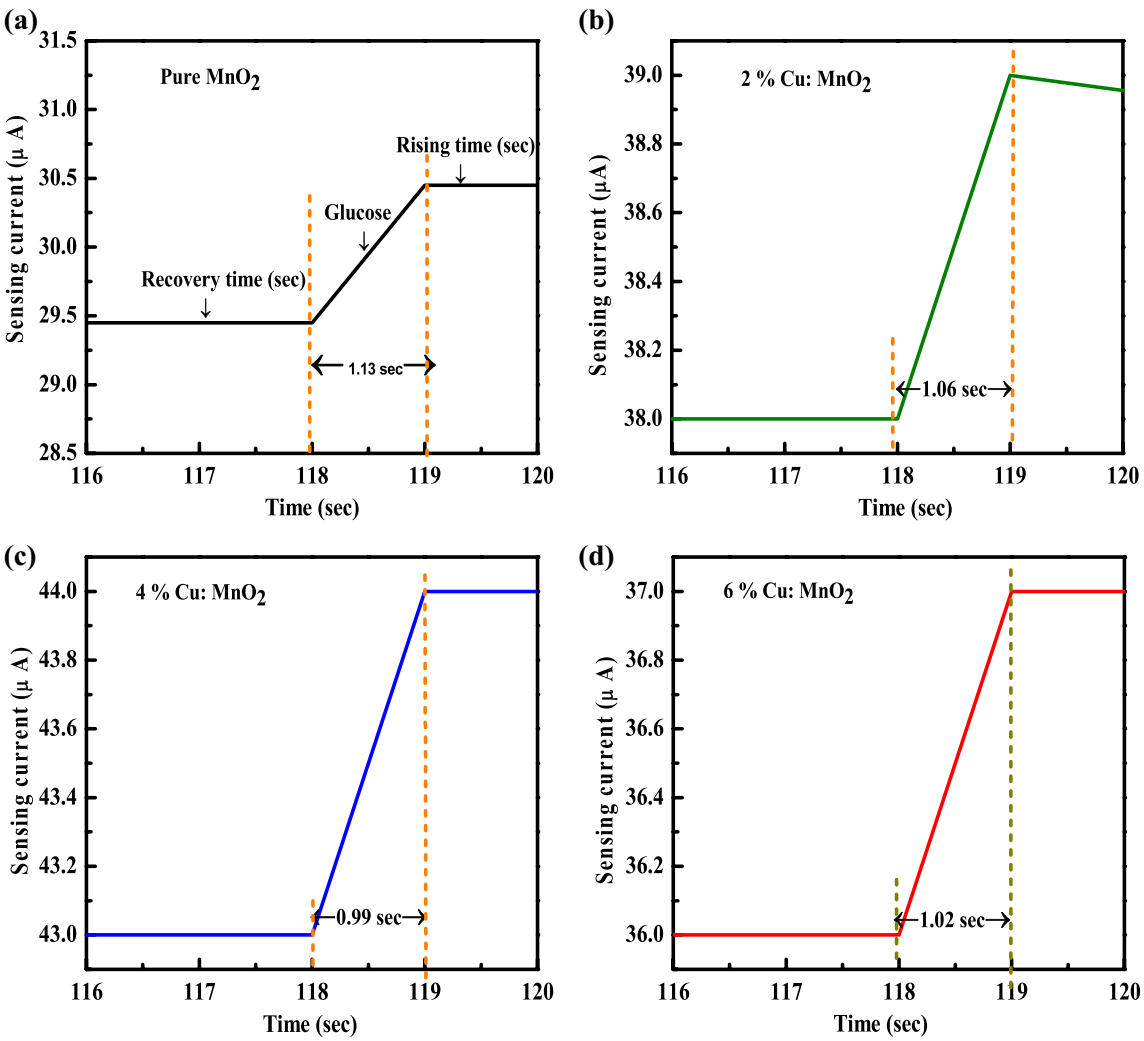

Fig. 8 **a**–**d** Response time of pure MnO_2 and 2, 4 and 6 at% Cu doped MnO_2

$$S = \frac{I_x}{I_g} \times 100$$

where I_x is the current underexposure and I_g is the current under ambient glucose. Figure 9a shows the glucose response of pure and 2, 4 and 6 at% Cu doped MnO_2 thin films variation with time. The response was dramatically increased with the increase of time and Cu concentration especially for 4 at% Cu higher than others shown in Fig. 9b.

3D views are shown in Fig. 10a–d has an ascending trend insensitivity of MnO_2 nanoparticles. In the 3D views, the blue color represents the direct recombination of conducting electrons, green color represents the recombination of surficial electron leading to visible emission. Red color represents the glucose sensitivity of pure MnO_2 and 2, 4, 6 at% Cu:MnO_2 thin films at 5 min existing 25–30% of all the films. In the red and violet region, the oxidation–reduction reaction occurred. Such images may due to the oxidation of glucose on the MnO_2. The oxidation is generated by deprotonating of glucose followed by adsorption onto the MnO_2 surface and oxidation by Mn^{+2} and Mn^{+4}. The Mn^{+4} ions are proposed to act as an electron-transfer medium [26]. First Mn^{+2} would be oxidized to Mn^{+4}. Then the oxidative Mn^{+4} could catalyze glucose oxidation to generate gluconolactone, and then gluconolactone is further oxidized to glucose acid shown as below

$$MnO_2 + OH \rightarrow MnOOH + 2e^-$$
$$MnOOH + 2e^- + \text{glucose}(C_6H_{12}O_6) \leftrightarrow MnO_2 + OH + \text{gluconic acid}$$

In the oxidation process Cu^{+1} and Mn^{+2} present in the Cu:MnO_2 electrode is converted into Cu^{+2} and Mn^{+4} by oxidation reaction, and these oxidation products are glucose, which can be rapidly oxidized to glucose lactone as bellow:

$$Cu^{+2} + C_6H_{12}O_6 \rightarrow Cu^{+1} + C_6H_{10}O_6,$$
$$Mn^{+4} + C_6H_{12}O_6 \rightarrow Mn^{+2} + C_6H_{10}O_6$$

The high sensitivity of 4 at% Cu:MnO_2 indicates the superior catalytic activity than pure MnO_2. Such high sensitivity may due to low crystallite size and high optical band gap shown in Fig. 10b. Figure 10c also shows that higher glucose sensitivity may due to higher carrier concentration. The sensitivity of the thin films prepared in this study is higher than those in previous reports of spin-coated or electrodeposited MnO_2 films [27, 28]. Figure 11a, b also indicates the correlation of sensitivity among average crystallite size, optical band gap and carrier concentration of pure MnO_2 and 2, 4 and 6 at% Cu:MnO_2 at 5 min and constant 0.5 mol/L glucose concentration. It is found that both of the sensitivities change exponentially which satisfies the results reported by Hartono et al. [29] and Kondo et al. [19].

4 Conclusions

In this paper, the surface morphology, structural, optical and electrical properties of Cu-doped MnO_2 thin films synthesized by the spray pyrolysis technique with different Cu concentrations are investigated. The surface homogeneity of the deposited films increases with Cu content due to the effect of friction among the charge carriers. XRD patterns indicated that the Cu ions replaced Mn ions without changing the tetragonal structure up to 4 at% Cu doping and the change in the structural phase of the film occurs at 6 at% Cu concentration. Crystallite size decreases from 25 to 12 nm with an increase of Cu concentration between 0

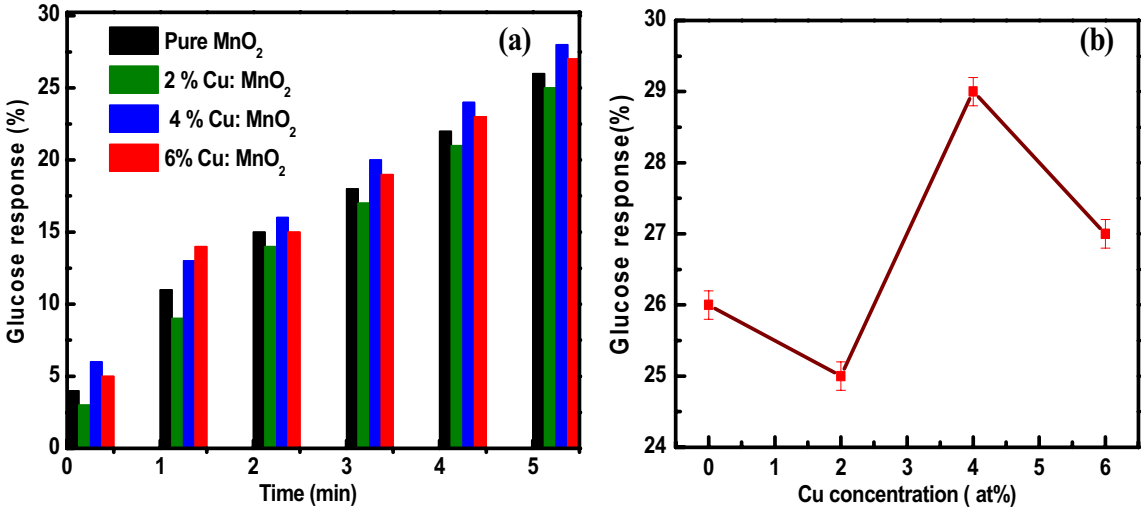

Fig. 9 Glucose sensitivity of pure MnO_2 and 2, 4, 6 at% Fe: MnO_2 thin films variation with time from 0 to 5 min

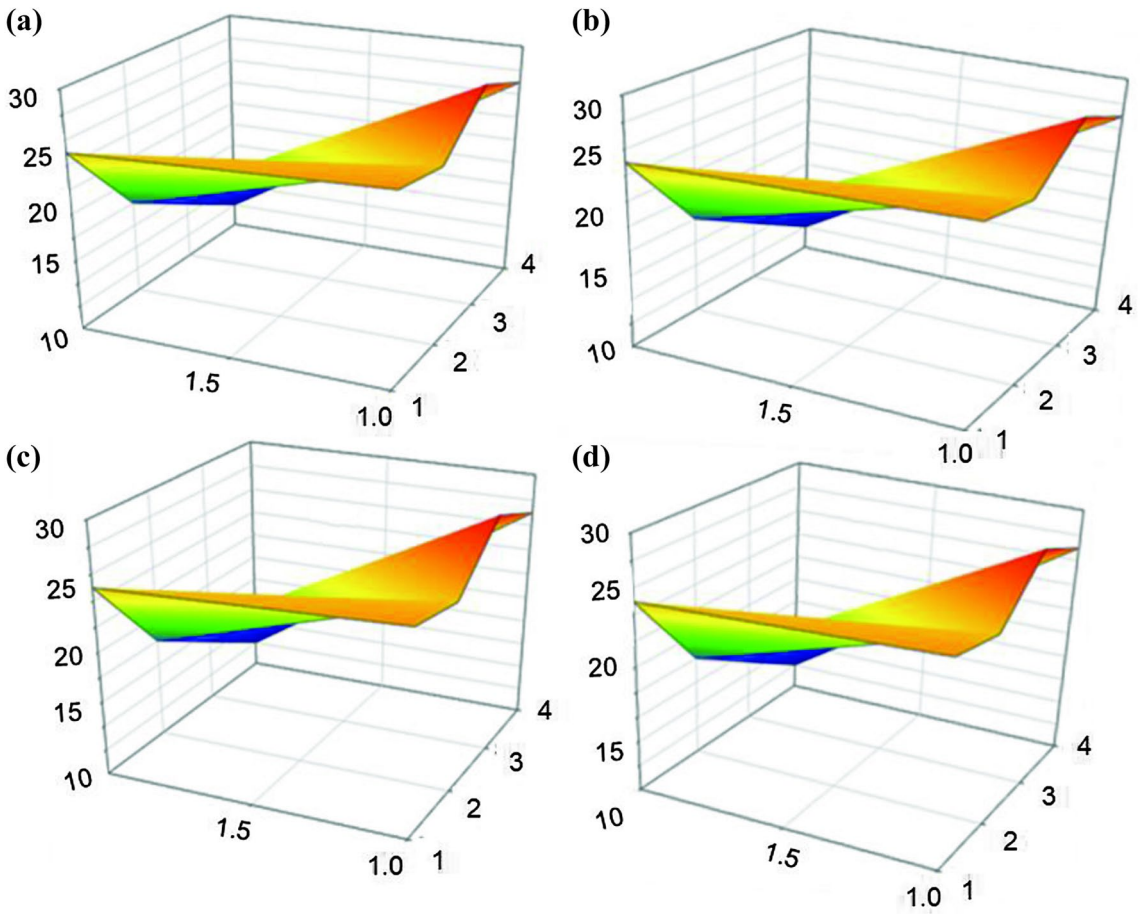

Fig. 10 **a**–**d** Glucose sensitivity of pure MnO_2 and 2, 4, 6 at% Cu:MnO_2 thin films at 5 min

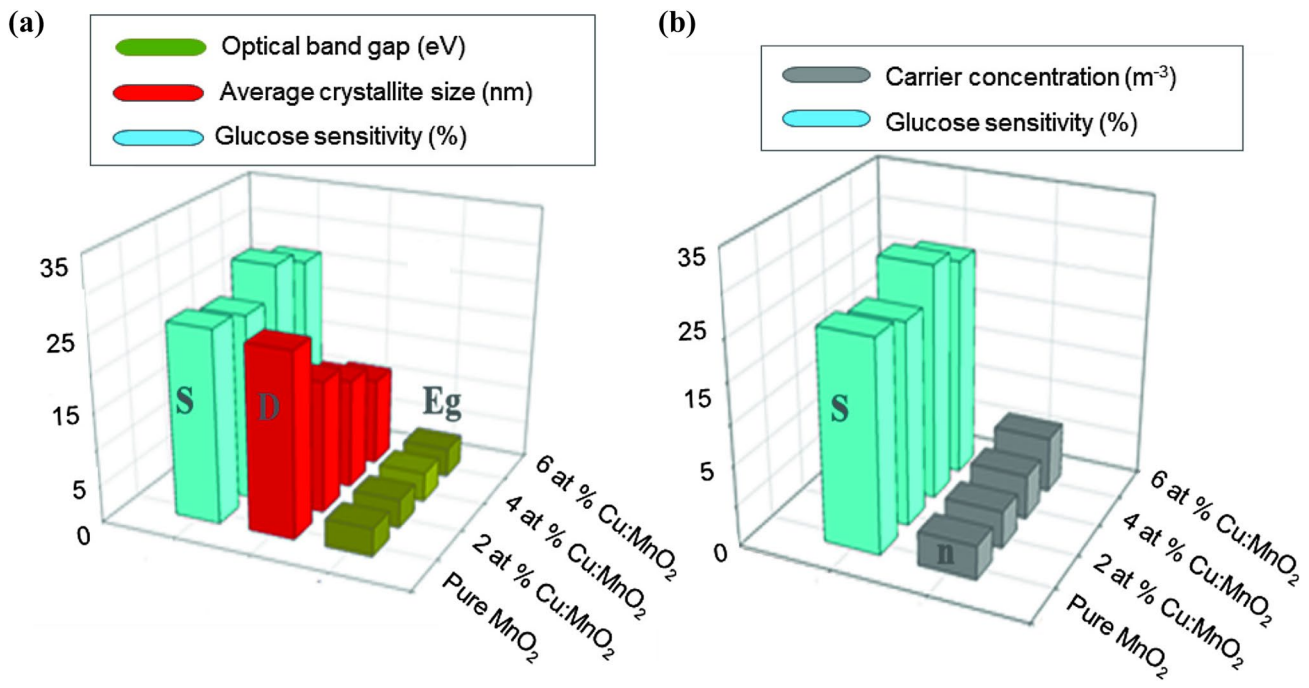

Fig. 11 **a**, **b** Correlation of sensitivity among average crystallite size, optical band gap and carrier concentration

to 6 at%. Cu-doped MnO_2 thin films are highly transparent in the visible-near-infrared region and the transmittance increases with increasing Cu concentration up to 4 at% reaching a maximum of 83%. The direct bandgap energy of the films rises between 3.82 to 3.96 eV with Cu concentration up to 4 at%. The electrical resistivity decreases with increasing Cu concentrations. Hall mobility and carrier concentration also increase with increasing Cu contents. Small crystallite size, the regularity of surface morphology, high transmittance, tunable bandgap, less resistivity, high carrier concentration and high mobility of Cu-doped MnO_2 thin films suggest the suitability of the material in optoelectronic devices and bio and gas sensing applications. Good sensitivity and response for 4 at% Cu:MnO_2 have been obtained. Spray deposited MnO_2 and Cu:MnO_2 thin films give the high specific surface area of the film layer as well as its firm adhesion to the substrate, which in turn contributed to the superior sensing abilities of the prepared films.

Acknowledgements One of the authors, Muslima Zahan is grateful to the Ministry of Science and Technology, Government of the People's Republic of Bangladesh for granting NST fellowship for her PhD. This publication is dedicated to the birth centenary of Bangabandhu Sheikh Mujibur Rahman, the 'Father of the Bangalee Nation'.

Compliance with ethical standards

Conflict of interest The authors declare that they have no conflict of interest.

References

1. Tian K, Prestgard M, Tiwari A (2014) A review of recent advances in nonenzymatic glucose sensors. Mater Sci Eng C 41:100–118
2. Marie M, Mandal S, Manasreh O (2015) An electrochemical glucose sensor based o zinc oxide nanorods. Sensors 15:18714–18723
3. Ahlers S, Muller G, Doll T (2005) A rate equation approach to the gas sensitivity of thin film metal oxide materials. Sensors Actuators B 107:587–599
4. Listorti A, Oregan B, Durrant R (2011) Electron transfer dynamics in dye-sensitized solar cells. Chem Mater 23:3381–3399
5. Qu Q, Wang B, Chen Y, Tian S, Wu Y, Holze R (2009) Electrochemical performance of MnO_2 nanorods in neutral aqueous electrolytes as a cathode for asymmetric supercapacitors. J Phys Chem C 113:14020–14027
6. Li Q, Sun X, Lozano K, Mao Y (2013) Asymmetric super capacitors with dominant pseudo capacitance based on manganese oxide nano flowers in a neutral aqueous electrolyte. RSC Adv 3:24886–24890
7. Shaban M, Abdelkarem K, Sayed AME (2019) Structural, optical and gas sensing properties of Cu_2O/CuO mixed phase: effect of the number of coated layers and (Cr + S) co-doping. Phase Transit 92:347–359
8. Liu Y, Wang N, Yao M, Yang C, Hu W, Komarneni S (2017) Porous Ag-doped MnO_2 thin films for supercapacitor electrodes. J Porous Mater 24:1717–1723
9. Tian Q, Wang X, Huang G, Guo X (2017) Nanostructured (Co, Mn)$_3O_4$ for high capacitive supercapacitor applications. Nanoscale Res Lett 12:214–220
10. Shaban M, Sayed AME (2015) Structural, optical and photocatalytic properties of fe and (Co, Fe) co-doped copper oxide spin coated films. Spectrochim Acta A Mol Biomol Spectrosc 149:638–646. https://doi.org/10.1016/j.saa.2015.05.010
11. Khmissi H, Sayed AME, Shaban M (2016) Structural, morphological, optical properties and wettability of spin-coated copper oxide; influences of film thickness, Ni, and (La, Ni) co-doping. J Mater Sci 51:5924–5938
12. Su X, Yu L, Cheng G, Zhang H, Sun M, Zhang L, Zhang J (2014) Controllable hydrothermal synthesis of Cu-doped α-MnO_2 films with different morphologies for energy storage and conversion using super capacitors. Appl Energy 134:439–445
13. Panić VV, Dekanski AB, Stevanović RM (2010) Sol-gel processed Thin-layer ruthenium oxide/carbon black supercapacitors: a revelation of the energy storage issues. J Power Sources 195(13):3969–3976
14. Tominaga S, Momma T, Scrosati B, Osaka T (2010) Sulfated zirconia as a proton conductor for fuel cells: stability to hydrolysis and influence on catalysts. J Power Sources 195:4065–4071
15. Njagi EC, Chena CH, Genuinoa H, Galindo H, Huang H, Steven, Suiba L (2010) Total oxidation of CO at ambient temperature using copper manganese oxide catalysts prepared by a redox method. Appl Catal B 99:103–110
16. Chtouki T, Louardi A, Elidrissi B, Taguig H (2013) Structural, morphological and optical properties of $Zn_xCo_{3-x}O_4$ ($0 \le x \le 1$) thin films prepared by spray pyrolysis technique. J Mater Sci Eng A 3:743–750
17. Rahman F, Zahan M, Podder J (2013) Synthesis of nanocrystalline ZnS thin films via spray pyrolysis for optoelectronic devices. Sensors Transducers 149:54–59
18. Wan X, Wang J, Zhu L, Tang J (2014) Gas sensing properties of Cu_2O and its particle size and morphology dependent gas-detection sensitivity. J Mater Chem A 2:13641–13647
19. Terukazu K, Yuta M, Keigo M, Hidero U (2018) Amperometric sensing of H_2O_2 and glucose using wet-chemicallydeposited MnO_2 thin films. J Ceram Soc Jpn 126:260–262
20. Forouhi AR, Bloomer I (1988) Optical properties of crystalline semiconductors and dielectrics. Phys Rev B 38:1865–1874
21. Cullity BD, Stock SR (2001) Elements of X-ray diffraction, 3rd edn. Prentice-Hall, New Jersey, p 664
22. Barret CS, Massalski TB (1980) Structure of metals: crystallographic methods, principles, and data. Pergamon Press, Oxford, p 204
23. Pishdadian S, Ghaleno AMS (2013) Influences of annealing temperature on the optical and structural properties of manganese oxide thin film by Zn doping from sol-gel technique. Acta Phys Pol A 123:9741–9745
24. Iligan S, Caglar M, Caglar Y (2007) The effect of deposition parameters on the physical properties of $Cd_xZn_{1-x}S$ films deposited by spray pyrolysis method. J Optoelectron Adv Mater 9:1414–1417
25. Zahan M, Podder J (2019) Surface morphology, optical properties and Urbach tail of spray deposited Co_3O_4 thin films. J Mater Sci Mater Electron 30:4259–4269. https://doi.org/10.1007/s10854-019-00717-2
26. Worsley GJ, Tourniaire GA, Medlock KES, Sartain FK, Harmer HE, Thatcher M (2007) Continuous blood glucose monitoring with a thin-film optical sensor. Clin Chem 53:1820–1826. https://doi.org/10.1373/clinchem.2007.091629
27. Baloch Q, Tahira A, Mallah AB, Abro MI, Uddin S et al (2016) A robust, enzyme-free glucose sensor based on lysine-assisted CuO nanostructures. Sensors 16:1878. https://doi.org/10.3390/s16111878

28. Zhang M, Liao C, Mak CH, You P, Mak CL, Yan F (2015) Highly sensitive glucose sensors based on enzyme-modified whole-graphene solution-gated transistors. Sci Rep 5:8311. https://doi.org/10.1038/srep08311
29. Hartono A, Sanjaya E, Ramli R (2018) Glucose sensing using capacitive biosensor based on polyvinylidene fluoride thin film. Biosensors 8:12. https://doi.org/10.3390/bios8010012